Journal of Magnetism and Magnetic Materials 587 (2023) 171304

Contents lists available at ScienceDirect

Journal of Magnetism and Magnetic Materials

journal homepage: www.elsevier.com/locate/jmmm

# Small zinc doped iron oxide tracers for magnetic particle imaging

H.T. Kim Duong [a], Ashkan Abdibastami [a], Lucy Gloag [a,*], Andre Bongers [b], Saeed Shanehsazzadeh [b], Melanie Nelson [c], Aidan Cousins [c], Narges Bayat [d,e,f], Hannah McCalmont [d,e,f], Richard B. Lock [d,e,f], Scott Sulway [a], Joanna Biazick [g], J. Justin Gooding [a,h], Richard D. Tilley [a,g,*]

[a] School of Chemistry, UNSW Sydney, NSW 2052, Australia
[b] Biological Resources Imaging Laboratory, Mark Wainwright Analytical Centre, UNSW Sydney, NSW 2052, Australia
[c] Ferronova Pty Ltd, Salisbury South, SA 5106, Australia
[d] Children's Cancer Institute Australia, Lowy Cancer Centre, UNSW Sydney, NSW 2052, Australia
[e] School of Women's and Children's Health, UNSW Sydney, NSW 2052, Australia
[f] University of New South Wales Centre for Childhood Cancer Research, UNSW Sydney, NSW 2052, Australia
[g] Electron Microscope Unit, Mark Wainwright Analytical Centre, UNSW Sydney, NSW 2052, Australia
[h] Australian Centre for NanoMedicine, UNSW Sydney, NSW 2052, Australia

A B S T R A C T

Magnetic particle imaging (MPI) has garnered significant attention in biomedical imaging research due to its excellent signal intensity that is generated directly from superparamagnetic iron oxide nanoparticles (SPIONs). Small nanoparticle tracers with high saturation magnetisation are crucial for MPI as they can prolong circulation, crossing the blood brain barrier and enhance cellular uptake. In this work, we demonstrate small zinc doped iron oxide nanoparticles (Zn-IONPs) are excellent MPI tracers. Our Zn-IONPs exhibited up to 37 % and 64% enhancement in saturation magnetisation (Msat) value and MPI signal intensity respectively compared to $Fe_3O_4$ of the same size. As a result, the polymer encapsulated Zn-IONPs achieved up to 2.7-fold enhancement in MPI signal intensity compared to VivoTrax. Furthermore, these polymer encapsulated NPs were also determined to be non-toxic hence making these Zn-IONPs ideal for many biomedical applications in MPI where small size is critical to prolong circulation time and crossing the blood brain barrier.

## 1. Introduction

Magnetic Particle Imaging (MPI) is a non-invasive imaging technology that detects magnetic nanoparticle (NP) tracers [1–6]. MPI can provide high quality images with no background signal and high sensitivity [5,7,8], which makes it an exciting new imaging modality that has the potential to become a quintessential diagnostic tool.

To achieve high quality MPI images with small tracers, NP cores need to have high saturation magnetisation ($M_{sat}$) that results in both high signal and high resolution [9]. Significant research has focused on improving magnetic properties of superparamagnetic iron oxide nanoparticles (SPIONs) of core size larger than 20 nm, because the $M_{sat}$ value is directly related to SPION size, i.e. larger SPIONs have larger MPI signal intensity [10–12]. However, larger NP size leads to a large hydrodynamic size after coating that can compromise biological performance [13,14]. Previous work by our group highlighted the potential of 14 nm Fe@$Fe_3O_4$ NPs as small MPI tracers. The use of more highly magnetic zero-valent Fe resulted in 3x greater $M_{sat}$ value than typical SPIONs of same size and achieved a similar MPI signal to VivoTrax [15]. There is an opportunity for the development of small tracers made of other highly magnetic materials to achieve even higher $M_{sat}$ and improved signal intensity in MPI to surpass standard tracers.

Doping SPIONs with zinc is known to enhance the magnetic properties of magnetite [16–18]. In magnetite, $Fe^{3+}$ ions located in tetrahedral sites have spins that are antiparallel to the spins from $Fe^{3+}$/$Fe^{2+}$ ions in octahedral sites. These tetrahedral ions counteract some of the magnetism and result in a $M_{sat}$ of 92 emu $g^{-1}$ in bulk [19]. Doping can boost the $M_{sat}$ as it can remove the opposing magnetic force from antiparallel spins and leads to an increase in $M_{sat}$ value. This can be achieved by the substitution of antiparallel $Fe^{3+}$ spins in the tetrahedral sites with a diamagnetic $Zn^{2+}$ spins and the final zinc doped iron oxide NPs adopts a normal spinel structure [16–18]. Due to its biocompatibility, zinc based materials have been widely studied for biomedical research [20]. Therefore, there is an opportunity to use zinc doped iron

* Corresponding authors at: School of Chemistry, UNSW Sydney, NSW 2052, Australia (R.D. Tilley); Mathematical and Physical Sciences, UTS, NSW 2007, Australia (L. Gloag).
*E-mail addresses:* lucy.gloag@uts.edu.au (L. Gloag), r.tilley@unsw.edu.au (R.D. Tilley).

https://doi.org/10.1016/j.jmmm.2023.171304
Received 18 May 2023; Received in revised form 13 September 2023; Accepted 21 September 2023
Available online 22 September 2023

oxide NPs (Zn-IONPs, also known as zinc ferrite NPs) as core material to produce small tracers with enhanced magnetic properties to further improving MPI performance. Here, we present Zn-IONPs with 11 nm and 15 nm cores as effective small tracers for MPI applications. The 11 nm and 15 nm Zn-IONPs were encapsulated with poly (maleic anhydride-*alt*-1-octadecene) polymer and achieved a small hydrodynamic size. The small tracers developed here exhibited compared to commercial tracers that are similar in size.

## 2. Experimental section

### 2.1. Chemicals and reagents

Iron (III) acetylacetonate ($Fe(acac)_3$, 99.9%), zinc chloride ($ZnCl_2$, 99.9%), oleic acid (90%), oleylamine (70%), trioctylamine (98%), benzyl ether (98%), poly (maleic anhydride-*alt*-1-octadecene) polymer (PMAO, $M_n$ 30,000–50,000), sodium hydroxide (NaOH, 98% pellets), chloroform ($CHCl_3$) and Dulbecco's phosphate buffered saline (DPBS) were purchased from Sigma Aldrich. Toluene and ethanol (absolute) were purchased from ChemSupply Pty Ltd Australia. Sodium hydroxide solution (NaOH, 2 M) were prepared with high purity Milli-Q water. RPMI-1640 growth medium was purchased from Gibco and supplemented with 20% foetal bovine serum (FBS) for MHH-CALL4 (CALL4) and 10% FBS for Nalm6 B-cell acute lymphoblastic leukemia (B-ALL) cell lines. Uranyl acetate and Resin-Procure 812 were purchased from Electron Microscopy Sciences (EMS) in USA. Diamond knife was purchased from Diatome in Switzerland. Osmium tetroxide was purchased from ProSciTech in Queensland. All solvents used for synthesis and purification were analytical grade.

### 2.2. Synthesis of 11 nm Zn-IONPs

In a typical synthesis of 11 nm Zn-IONPs, $Fe(acac)_3$ (424 mg, 1.2 mmol) and $ZnCl_2$ (120 mg, 0.88 mmol) were added into a 50 mL multi-neck round bottom flask with a mixture of oleylamine (4.8 mL), oleic acid (1.2 mL) and trioctylamine (4.8 mL). The mixture was sonicated and stirred magnetically on a hotplate. The reaction mixture was degassed at 120 °C for 90 min. Then argon gas was incorporated into the system and the temperature was gradually increased to 250 °C (5 °C/min) and maintained at this temperature for 2 h. Finally, the temperature was gradually increased to 350 °C (2 °C/min) and maintained at this temperature for 50 min. The reaction mixture was allowed to cool down and the black solution was transferred into a falcon centrifuge tube. Ethanol (EtOH, 30 mL) and toluene (8 mL) were added into the solution. The black precipitate was collected *via* centrifugation after 5 min at 1600 rcf. Toluene (8 mL) and oleylamine (30 mL) were added to disperse the NPs and supernatant was collected *via* centrifugation after 3 min at 650 rcf. Finally, EtOH (4 mL) was added, and the black precipitate was collected after 5 min of centrifugation at 1600 rcf. The 11 nm Zn-IONPs were suspended in toluene (2 mL) and stored at room temperature for further characterisations.

### 2.3. Synthesis of 15 nm Zn-IONPs

The synthetic procedure was the same as for 11 nm Zn-IONPs but the time for the reaction to take place at 350 °C was maintained for 4 h before cooling and purifying.

### 2.4. Synthesis of 11 nm magnetite IONPs

In a typical synthesis of 11 nm $Fe_3O_4$ NPs, $Fe(acac)_3$ (735 mg, 2.08 mmol) was added into a 50 mL multi-neck round bottom flask with a mixture of benzyl ether (10 mL) oleylamine (1.2 mL) and oleic acid (1.22 mL). The mixture was sonicated and stirred magnetically on a hotplate. The reaction mixture was degassed at 120 °C for 90 min. Then argon gas was incorporated into the system and the temperature was gradually increased to 200 °C (5 °C/min) and maintained at this temperature for 2 h. Finally, the temperature was gradually increased to 300 °C (2 °C/min) and maintained at this temperature for 1 h. The reaction mixture was allowed to cool down and the black solution was transferred into a falcon centrifuge tube. Ethanol (EtOH, 30 mL) and toluene (8 mL) were added into the solution. The black precipitate was collected *via* centrifugation after 5 min at 1600 rcf. Toluene (8 mL) and oleylamine (30 mL) were added to disperse the NPs and supernatant was collected *via* centrifugation after 3 min at 650 rcf. Finally, EtOH (4 mL) was added, and the black precipitate was collected after 5 min of centrifugation at 1600 rcf. The 11 nm $Fe_3O_4$ NPs were suspended in toluene (2 mL) and stored at room temperature for further characterisations.

### 2.5. Synthesis of 15 nm magnetite IONPs

The synthetic procedure was the same as for 11 nm magnetite IONPs but the time for the reaction to take place at 350 °C was maintained for 4 h before cooling and purifying.

### 2.6. Polymer encapsulation of Zn-IONPs with poly (maleic anhydride-alt-1-octadecene) (PMAO)

In a typical PMAO encapsulation of NPs, Zn-IONPs sample (30 mg) was transferred into a sample glass vial and was redispersed with $CHCl_3$ (1 mL) with sonication. In a separate glass vial, PMAO (300 mg) and $CHCl_3$ (2.7 mL) were added and sonicated until all PMAO was dissolved. PMAO solution was then transferred into the NPs suspension and was sealed with parafilm. The NPs mixture was stirred using a table shaker for 48 h. The solution was then dried with rotary evaporator and NaOH (2 M, 7.2 mL) was added. The solution was stirred at 80 °C under 600 mbar until a successful phase transfer from organic to aqueous was achieved. The PMAO coated Zn-IONPs was purified using centrifugation at 14,000 rpm for 3 h and followed by magnetic cleaning. Finally, the magnetic cleaning step was repeated two more times and the PMAO coated NPs were suspended in DPBS (3 mL) for long-term storage.

### 2.7. Sterilisation of polymer coated NPs

An aliquot of polymer coated Zn-IONPs (1 mL) was transferred into a 20 mL sample glass vial and diluted in Milli-Q water (10 mL). The NPs suspension was sterilised with UV radiation for 1 h to kill all the bacteria and filtered in sterile condition with a syringe filter (0.22 μm). Then it was transferred into an autoclaved centrifuge tube and the NP precipitates were collected with centrifugation at 14,000 rpm after 3 h and redispersed in sterile DPBS for cell toxicity assay and analysis.

### 2.8. Cell apoptosis assays

Cell apoptosis assays using allophycocyanin (APC)-labelled Annexin V and 7-aminoactinomycin D (7AAD) viability stain (BD Biosciences) were conducted to ensure biocompatibility of the NPs. Two human B-ALL cell lines, Nalm6 and CALL4, with doubling times of approximately 36 h and 90 h, respectively, were selected to assess the impact of cellular proliferation rate on uptake of the NPs. Briefly, Nalm6 and CALL4 were seeded at optimised cell seeding densities of 0.7 M cells/mL and 0.3 M cells/mL, respectively, and incubated with 10 mg/L of solution containing 11 nm or 15 nm PMAO coated Zn-IONPs dispersed in DPBS. Cells were either washed after 1 h or allowed to incubate with the NPs for 4 or 24 h. Following incubation, cells were washed 3 times with DPBS and residual NPs removed from solution using a magnetic separator (Invitrogen). Finally, cells were double stained with Annexin V and 7AAD and resuspended in DPBS for flow cytometric analysis using a FACSCanto flow cytometer (BD Biosciences) to determine the proportion of viable cells. The experiment was conducted in triplicate and cell viability expressed as a percentage of the DPBS-treated control.

### 2.9. Characterisations

#### 2.9.1. Transmission electron microscopy (TEM)

TEM images were recorded on a FEI Tecnai G2 20 TEM. 2 drops of NP solution were placed onto a carbon-coated copper grid and dried at room temperature. Elemental mapping of zinc and iron in synthesised NPs was confirmed by energy dispersive X-ray spectroscopy (EDX; JEOL JEM-F200).

#### 2.9.2. Inductively coupled plasma optical emission spectroscopy (ICP-OES)

The iron and zinc concentrations were quantified using inductively coupled plasma optical emission spectroscopy (ICP-OES; Optima7000 PerkinElmer). NP solution (100 mL) were added into a sample glass vial and dried under nitrogen gas. The dried NP was dissolved using *aqua regia* (2 mL) and the acid solution was heated at 80 °C for 1 h to facilitate the digestion of NPs. The solution was diluted 10 times with Milli-Q water and submitted to ICP-OES for determination of Fe and Zn content.

#### 2.9.3. X-ray diffraction (XRD)

XRD characterisation was performed using a PANalytical X'Pert Multipurpose X-ray Diffractometer (MPD) with Cu-Kα radiation (1.5406 Å) operating at 45 kV and 40 mA. Data were collected from 15° to 100° 2θ, step size 0.013° and time per step of 350 s at room temperature. The beam pass was defined using a 1/2 divergence slit, 10 mm mask, and 1 anti-scatter slit.

#### 2.9.4. Vibrating sample magnetometer (VSM)

Magnetic characterisation was performed with a Quantum Design MPMS3 superconducting interference Device (SQUID). The field-dependent magnetic properties of samples were studied by using VSM. All samples were subjected to a constant frequency of 40 Hz. Hysteresis loops were registered at 300 °K as the magnetic field is cycled between −30 and 30 kOe with ramp rate of 50 Oe per second. VSM analysis was performed on a sample of dried zinc doped iron oxide NPs containing 0.71 mg and 0.78 mg of total mass of inorganic nanoparticle core for 11 nm and 15 nm respectively.

#### 2.9.5. Magnetic particle imaging (MPI)

The MPI performance of NPs was evaluated using 2D projection scan through a Magnetic Insight, Inc., MOMENTUM pre-clinical scanner. Samples were individually scanned using the RELAX™ module equipped on the MOMENTUM™ imager to produce a point spread function (PSF) for each sample. Images were acquired in 2D with a 5.7 T/m selection field gradient and excitation field strengths of 20 and 26 mT in the X and Z channels, respectively. All the samples were subjected with a constant frequency of 45 kHz in the MPI scanner. These 2D images took ~ 2 min to acquire for a 12 × 6 cm field of view (FOV). A stock solution of NP solution with the concentration of 0.1 mg/mL of Fe was prepared and the concentration was determined by using ICP-OES. Five different concentrations were made using the 0.1 $mg_{Fe}$/mL stock solution to have Fe concentrations ranging from 5 μg/mL to 100 μg/mL. MPI measurements were performed on both oleic coated and polymer coated NPs.

#### 2.9.6. Analysis of NPs internalisation into cells

TEM analysis was conducted to confirm the uptake and internalisation of Zn-IONPs by the Nalm6 and CALL4 cell lines. After 24 h incubation, the cells-NPs were fixed in 2.5% (w/v) glutaraldehyde in 0.2 M sodium phosphate buffer at 4 °C overnight. Fixed samples were rinsed with 0.1 M sodium phosphate buffer and post fixed in 1% osmium tetroxide in 0.2 M sodium buffer by using a BioWave Pro + Microwave Tissue Processor (Ted Pella, USA). After rinsing with 0.1 M sodium phosphate buffer, samples were dehydrated in a graded series of ethanol, infiltrated with resin (Procure, 812), and polymerised using an oven at 60 °C for 48 h. Ultrathin sections (70 nm) were cut using a diamond knife (Diatome) and collected onto carbon-coated copper slot TEM grids. Grids were post-stained using uranyl acetate (2%) and lead citrate. Two grids were collected from duplicate regions for each sample and imaged using a JEOL 1400 TEM (Tokyo, Japan) operating at 100 kV.

## 3. Results and discussion

The zinc doped iron oxide NPs were synthesised *via* thermal decomposition method adapted from nature protocol [17]. By controlling the molar ratio of iron to zinc to be 1:1.36, Zn-IONPs with 13% zinc content was successfully obtained (determined by ICP and EDX). This composition was chosen as it was previously been reported in literature that gives zinc doped magnetite NPs the highest $M_{sat}$ value [16,17].

High-resolution transmission electron microscopy (HR-TEM) images of these Zn-IONPs confirmed the even distribution of zinc across the NPs, as shown in Fig. 1c and f, with a zinc content of approximately 13% which matches the ICP results. This gives an overall formula of $Zn_{0.4}Fe_{2.6}O_4$ which is the optimal composition to achieve the highest $M_{sat}$ [16–18]. The NPs were determined to be single crystalline as shown by the observation of lattice fringes with no defects over entire NPs (Fig. S1, ESI). In addition, X-ray diffraction (XRD) analysis of the magnetite and Zn-IONPs were also performed to confirm the crystal size and crystal structure of the NPs. The size calculated by using the

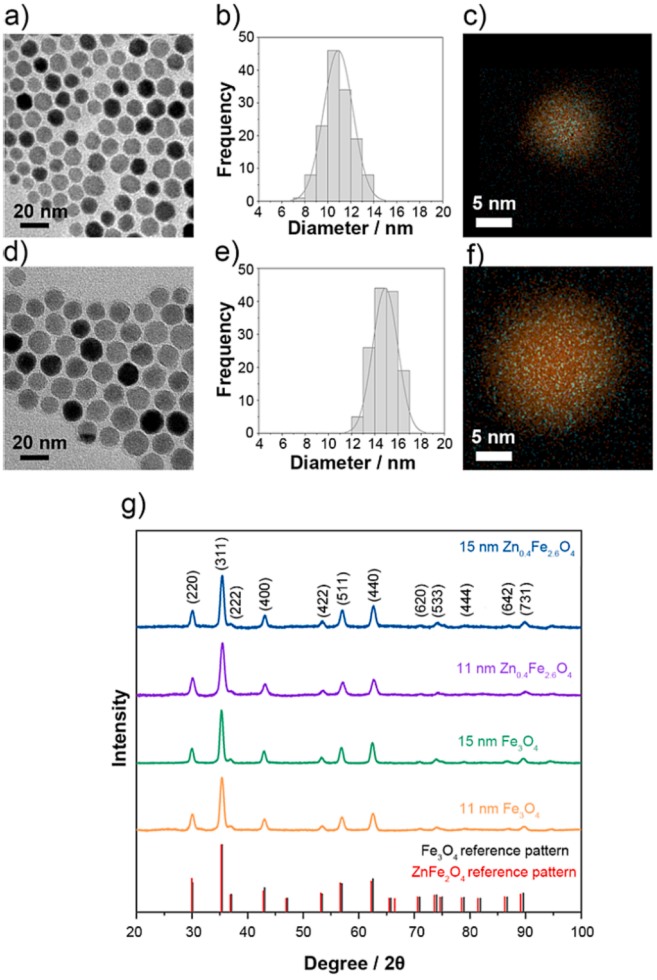


**Fig. 1.** Characterisation of two different sizes Zn-IONPs. Low-resolution transmission electron microscope (LR-TEM) images of 11 nm (**a**) with histogram showing the size distribution (**b**) and 15 nm (**d**) with histogram showing the size distribution (**e**). Energy dispersive x-ray (EDX) mapping of 11 nm (**c**) and 15 nm (**f**) obtained from high-resolution transmission electron microscopy (HR-TEM). X-ray diffraction (XRD) patterns were also obtained for 11 nm and 15 nm Zn-IONPs and compared to the iron oxide NPs of the same size as well as the $Fe_3O_4$ and $ZnFe_2O_4$ reference pattern (**g**).

Scherrer equation is 11 nm and 14 nm for Zn-IONPs which matches the size measured by LR-TEM. Fig. 1 g also shows that diffraction pattern for magnetite and Zn-IONPs for 11 nm and 15 nm samples. The crystal structure of the samples was determined to be zinc doped magnetite NPs as the peaks matched the standard reference patterns. The presence of peaks at indexed (220), (311), (400), (422), (511) and (440) reflection planes in the XRD pattern corresponds to the inverse spinel structure of zinc ferrite reference patterns [21].

Magnetic hysteresis of oleic acid (OA) coated Zn-IONPs were measured and compared to iron oxide magnetite NPs of the same size. Magnetic measurements were performed on dried powder of OA coated Zn-IONPs containing 0.71 mg and 0.78 mg of NPs for 11 nm and 15 nm respectively. The hysteresis loop shows that both 11 nm and 15 nm Zn-IONPs display superparamagnetic behaviour (Table S1) with coercivity of $< 2.5$ Oe. The saturation magnetisation ($M_{sat}$) of the nanoparticles was normalised against the inorganic nanoparticle mass in the sample (determined by ICP-OES) for easy comparison across literatures. We also provided the hysteresis loop normalising the magnetic measurements of Zn-IONPs against Fe + Zn mass as well as the mass of Fe in the ESI (S3, ESI) for comparison with other articles that use these normalisations. The $M_{sat}$ value for these oleic acid coated Zn-IONPs was determined to be approximately 91 emu/$g_{NPs}$ and 85 emu/$g_{NPs}$ for 11 nm and 15 nm NPs respectively (1 T = 10 kOe). These magnetisation values are in agreement with literature for Zn-IONPs of similar sizes [16]. After substituting 13% iron with zinc, the Zn-IONPs were shown to possess a much higher $M_{sat}$ value compared to magnetite NPs of same size. There was a 37% and 30% enhancement in magnetisation for 11 nm and 15 nm respectively (Fig. 2a). Since $Fe^{3+}$ and $Zn^{2+}$ have 5 and 0 unpaired valence electrons in d-orbitals respectively, any replacement of $Fe^{3+}$ in $T_h$ sites with $Zn^{2+}$ results in a significant decrease in the spin magnetic moment. The fall in spin magnetic moments on $T_h$ sites that are aligned antiparallel to the direction of the external magnetic field leads to an increase in the overall magnetic moment and in turn an increase in the $M_{sat}$.

The MPI performance of Zn-IONPs were assessed to study the influence of Zn-doping on the MPI signal intensity. Measurements were performed on OA coated Zn-IONPs and magnetite samples containing Fe concentrations ranging from 5 – 100 μg/mL in toluene, which is the range where no distortion from magnetic blooming was observed. Furthermore, we chose to normalise the MPI signal intensity of Zn-IONPs against Fe concentration to match the style reported in literature and make comparison easier. We also obtained the MPI and VSM measurements of oleic acid coated Zn-IONPs and magnetite NPs as dried powders to compare to their behaviour in the same state. The dried NPs exhibit broader signals and lower MPI signal intensities (see Fig. S4, ESI) than in solution samples, due to nanoparticle to nanoparticle interaction. All samples demonstrated a linear relationship between Fe mass and MPI signal with no loss of signal at low or high Fe mass. The $Zn_{0.4}Fe_{2.6}O_4$ NPs exhibited a higher MPI signal compared to magnetite NPs of the same size with a 64% and 58% improvement for 11 nm and 15 nm respectively. Interestingly, the 11 nm Zn-IONPs exhibited similar MPI signals as 15 nm $Fe_3O_4$ despite possessing different $M_{sat}$ value. In a very basic (adiabatic) Langevin magnetisation model, the saturation magnetisation as measured in VSM should directly correlate with MPI performance (i.e., peak MPI signal amplitude). Hence, MNPs with similar MPI performance should have the same or similar $M_{sat}$ value in VSM. This discrepancy may be due to other factors of MNPs such as effective core size, size distribution and magnetic anisotropy that may influence their MPI performance [22,23]. The other possible known causes for this discrepancy is the reduction of magnetization with increasing frequency. This can be explained as the inability of MNPs to closely follow the saturation curve when the frequency used in MPI scanner is too high as there is a considerable change in relaxation time. In order to confirm this, a plot showing the frequency dependence of susceptibility under alternating magnetic field need to be obtained. Unfortunately, the frequency of our MPI scanner is bound to 45 kHz hence it is difficult to test the frequency dependence. However, we are currently in the process of building a micro MPI relaxometer that can overcome these restrictions in the near future.

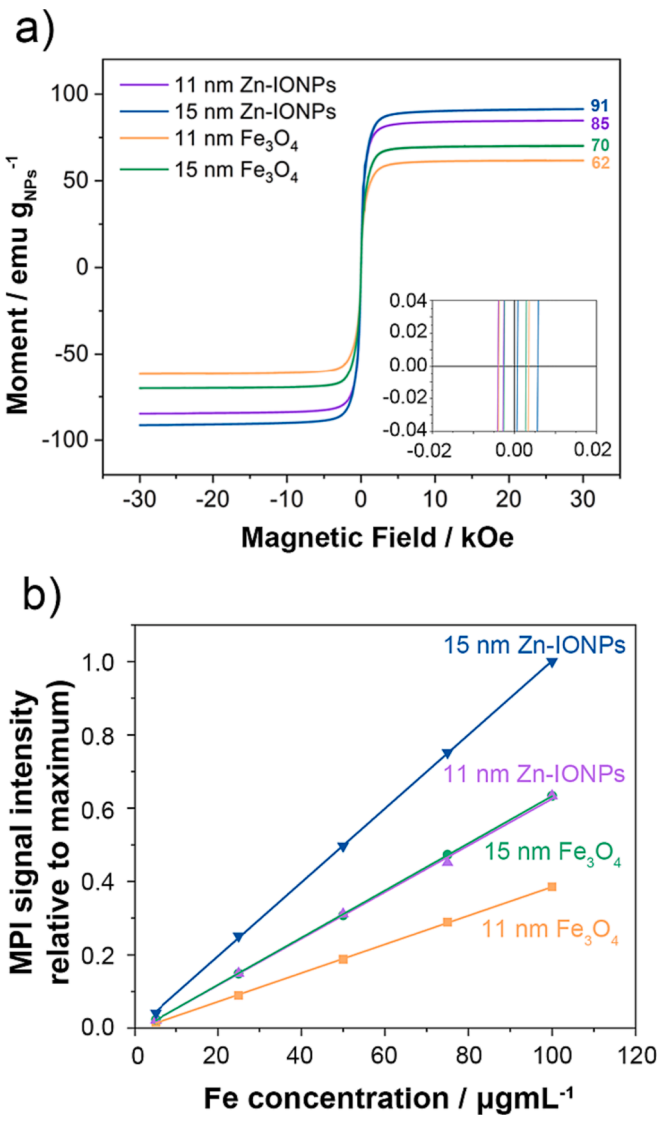


**Fig. 2.** Characterisations of the magnetic properties and MPI performance of uncoated Zn-IONPs. Hysteresis loop of 11 nm and 15 nm Zn-IONPs and 11 nm and 15 nm magnetite NPs at 300 K using vibrating sample magnetometer (VSM) (**a**). MPI measurements of Zn-IONPs (11 nm and 15 nm) and magnetite (11 nm and 15 nm) at different Fe concentrations (0 μg/mL – 100 μg/mL) (**b**) measured with 2D projection scan in MPI.

The Zn-IONPs were made water dispersible by encapsulating with a poly (maleic anhydride-*alt*-1-octadecene) (a.k.a. PMAO) polymer. The PMAO polymer was coated on the NPs *via* dispersion force between the long carbon chain of the oleic acid-NPs and the octadecene chain of the polymer (Scheme 1). Then 2 M NaOH was added to facilitate maleic anhydride ring opening to ensure the PMAO coated NPs had high water-dispersity and solubility. Fourier-transform infrared (FTIR) spectra of the Zn-IONPs before and after coating showed the successful phase transfer from organic to aqueous solvent (Fig. 3d). The PMAO polymer provides high colloidal stability, with the NPs remain dispersed in aqueous media for more than 12 weeks. The hydrodynamic size of the two polymer-coated Zn-IONPs were determined to be 55 nm (PDI = 0.193) for 11 nm NPs and 58 nm (PDI = 0.172) for 15 nm NPs. The small hydrodynamic size of the Zn-IONPs (less than 60 nm) is crucial for long circulation time *in vivo* and enable their uses in various applications such

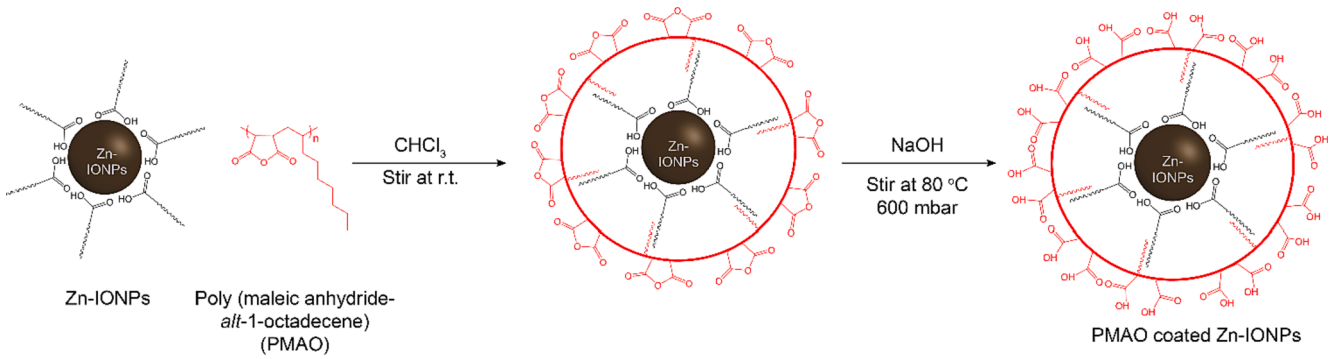


**Scheme 1.** Scheme illustrating the polymer encapsulation of Zn-IONPs with poly (maleic anhydride-alt-1-octadecene) (PMAO) polymer.

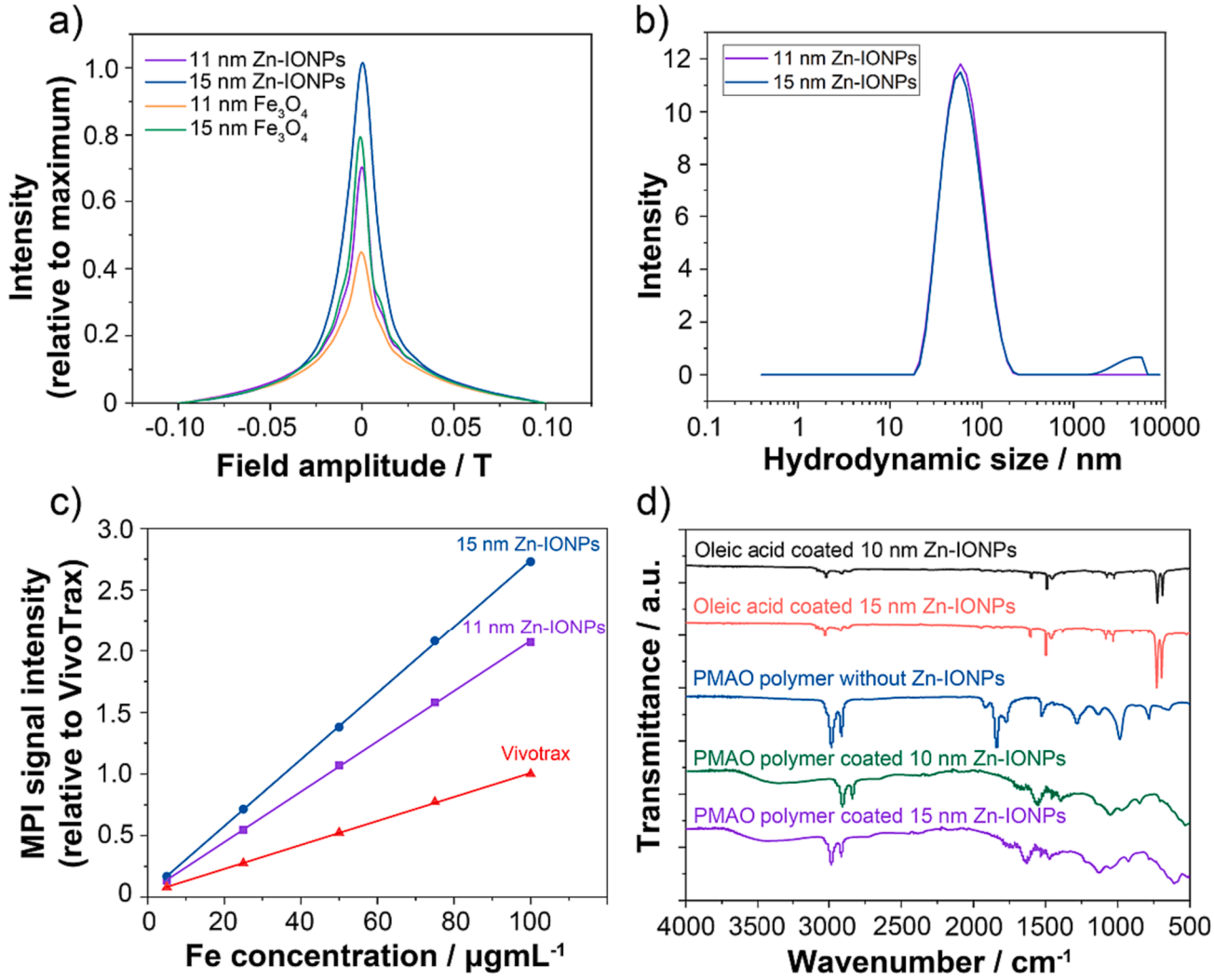


**Fig. 3.** Point spread function (PSF) curve of oleic acid coated Zn-IONPs and magnetite NPs (**a**). Dynamic light scattering (DLS) of polymer coated 11 nm and 15 nm Zn-IONPs (**b**). MPI measurements of 11 nm and 15 nm Zn-IONPs compared to VivoTrax at 5 mg/mL – 100 mg/mL of Fe concentration (**c**). Fourier Transform Infrared spectra of the zinc doped iron oxide nanoparticles before and after coating (**d**).

as long-term cellular tracking and labelling. These Zn-IONPs possess similar hydrodynamic size as VivoTrax, a commercial tracer that consists of 45–60 nm dextran coated clusters of 3–5 nm core IONPs. This enables us to investigate the effect of magnetic material composition on the MPI signal.

The performance of these Zn-IONPs as MPI tracers was assessed with magnetic particle spectroscopy (MPS) by comparing the MPI signals of these PMAO coated Zn-IONPs with commercial VivoTrax. The measurements were performed on the solution of PMAO coated Zn-IONPs and VivoTrax in water with concentration ranging from 5 to 100 μg/mL. MPI signals of the Zn-IONPs samples also demonstrated a linear relationship between Fe mass and MPI signal with no loss of signal at low or high Fe mass. The $Zn_{0.4}Fe_{2.6}O_4$ NPs exhibited a higher MPI signals compared to VivoTrax with approximately 2.1- and 2.7-fold

improvement for 11 nm and 15 nm respectively (Fig. 3c). Significantly, this is the highest MPI signals reported for tracers of less than 20 nm core materials [16,24–26], making these PMAO coated Zn-IONPs with hydrodynamic size less than 60 nm ideal for MPI applications such as cellular tracking and labelling, leukemia, hyperthermia and dementia studies.

The physicochemical properties of NPs, including size and surface coatings, as well as exposure conditions and incubation time may govern their cellular toxicity and uptake. Therefore, to assess the impact of the cellular proliferation rate on the uptake of PMAO encapsulated Zn-IONPs, two human B-cell ALL cells lines, Nalm-6 and CALL4, with different growth rates were selected for this study. We chose two acute lymphoblastic leukemia (ALL) cell lines, the Nalm6 and the CALL4 cell line, because they are leukemic cancer cells that associated with minimal residual disease (MRD) and treatment failure. This allowed us to gain a broader understanding of the cytotoxic effects of PMAO-coated Zn-IONPs in various ALL contexts and determine the suitability of these NPs in detecting MRD using MPI. Also, the two cell lines have different proliferation rates which would impact the uptake of the NPs. In this study, a concentration of 10 mg/L was chosen as a starting point for assessing the cytotoxicity and biocompatibility of the iron oxide nanoparticles. The rationale for using only one exposure concentration in the current study was to establish a baseline for understanding of the nanoparticles' biological effects across a range of exposure conditions including exposure duration (4 h, and 24 h), continuous exposure or washing away nanoparticles, and cellular proliferation rate. The cells were treated with different sizes (11 nm and 15 nm) of 10 mg/L of PMAO coated Zn-IONPs dispersed in DPBS at short exposure of 4 h and long exposure of 24 h. This allowed us to determine if the toxicity of these tracers is size or time dependent. The results showed that both 11 nm and 15 nm Zn-IONPs exhibited no toxic response towards Nalm6 and CALL4 cells at either 4 or 24 h exposure and $>$ 90% cell viability was observed (Fig. 4). Additionally, these 11 nm and 15 nm Zn-IONPs were well encapsulated within the cells as seen in the TEM images in Fig. 4. This confirms the biocompatibility of these Zn-IONPs as they induced no toxic response after being internalised by the cells. Therefore, this suggests the potential use of these Zn-IONPs tracers in future *in vivo* applications including imaging of cancer cells.

## 4. Conclusions

In this work, we have demonstrated that small sized NPs that possess excellent MPI performance can be achieved using Zn-IONPs. By substituting 13% $Fe^{2+/3+}$ with $Zn^{2+}$, Zn-IONPs achieved up to 37% and 64% enhancement in $M_{sat}$ and MPI, respectively, compared to magnetite NPs of the same size. As a result, the PMAO coated Zn-IONPs with hydrodynamic size of less than 60 nm achieved 2.1- and 2.7-fold improvement in MPI signal intensity for core size of 11 nm and 15 nm, respectively, compared to commercial VivoTrax. With the small size and high MPI performance, these Zn-IONPs will be more effective MPI tracers in prolonging blood circulation time, enhancing cellular uptake and crossing the blood brain barrier, which is crucial for applications such as hyperthermia, cellular tracking, dementia and leukemia studies.

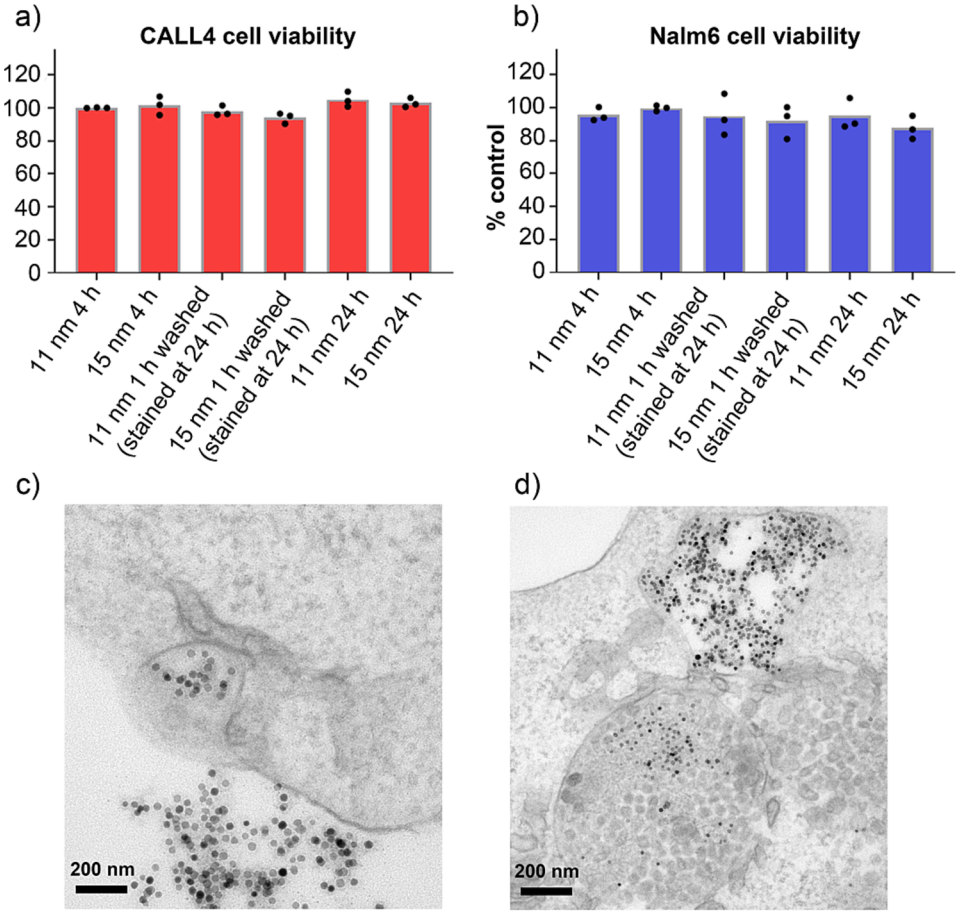


**Fig. 4.** Cell viability assay of 11 nm and 15 nm Zn-IONPs. Flow cytometry assay of 11 nm and 15 nm Zn-IONPs with CALL4 cell line at two timepoints (4 h and 24 h) (**a**). Flow cytometry assay of 11 nm and 15 nm Zn-IONPs with Nalm6 cell line at two timepoints (4 h and 24 h) (**b**). All toxicity assays were performed using 10 $mg_{Fe+Zn}$ /L nanoparticle solution. TEM images of the PMAO polymer coated 15 nm Zn-IONPs being internalised by the Nalm6 cell line (**c**) and (**d**).

## Declaration of Competing Interest

The authors declare that they have no known competing financial interests or personal relationships that could have appeared to influence the work reported in this paper.

## Data availability

Data will be made available on request.

## Acknowledgements

R. D. T. acknowledges the Australian Research Council Discovery Project DP200100143 and ARC Training Centre for Next-Gen Technologies in Biomedical Analysis IC210100056. J. J. G. acknowledges funding from The National Health and Medical Research Council of Australia (NHMRC Investigator Grant GNT1196648 and NHMRC Program Grant APP1091261). R. B. L. acknowledges funding from The National Health and Medical Research Council of Australia (NHMRC Fellowship APP1157871 and NHMRC Program Grant APP1091261). This research used facilities supported by Microscopy Australia at the Electron Microscope Unit in the Mark Wainwright Analytical Centre (MWAC) at UNSW. Children's Cancer Institute Australia is affiliated with UNSW Sydney and The Sydney Children's Hospitals Network.

## Appendix A. Supplementary data

Supplementary data to this article can be found online at https://doi.org/10.1016/j.jmmm.2023.171304.

## References

[1] P.M. Ferguson, et al., Strongly magnetic iron nanoparticles improve the diagnosis of small tumours in the reticuloendothelial system by magnetic resonance imaging, PLoS One 8 (2013) 1–7.
[2] H. Arami, et al., Invivo multimodal magnetic particle imaging (MPI) with tailored magneto/optical contrast agents, Biomaterials 52 (2015) 251–261.
[3] Q. Gao, et al., PLA2-responsive and SPIO-loaded phospholipid micelles, Chem. Commun. 51 (2015) 12313–12315.
[4] H. Arami, et al., Tomographic magnetic particle imaging of cancer targeted nanoparticles, Nanoscale 9 (2017) 18723–18730.
[5] E.Y. Yu, et al., Magnetic particle imaging: a novel in vivo imaging platform for cancer detection, Nano Lett. 17 (2017) 1648–1654.
[6] A.P. Khandhar, R.M. Ferguson, H. Arami, K.M. Krishnan, Monodisperse magnetite nanoparticle tracers for in vivo magnetic particle imaging, Biomaterials 34 (2013) 3837–3845.
[7] B. Gleich, J. Weizenecker, Tomographic imaging using the nonlinear response of magnetic particles, Nature 435 (2005) 1214–1217.
[8] G. Song, et al., Janus iron oxides @ semiconducting polymer nanoparticle tracer for cell tracking by magnetic particle imaging, Nano Lett. 18 (2018) 182–189.
[9] H.T.K. Duong, et al., A guide to the design of magnetic particle imaging tracers for biomedical applications, Nanoscale 14 (2022) 13890–13914.
[10] S. Liu, et al., Long circulating tracer tailored for magnetic particle imaging, Nanotheranostics 5 (2021) 348–361.
[11] R.M. Ferguson, et al., Magnetic particle imaging with tailored iron oxide nanoparticle tracers, IEEE Trans. Med. Imaging 34 (2015) 1077–1084.
[12] A.P. Khandhar, et al., Evaluation of PEG-coated iron oxide nanoparticles as blood pool tracers for preclinical magnetic particle imaging, Nanoscale 9 (2017) 1299–1306.
[13] N. Hoshyar, S. Gray, H. Han, G. Bao, The effect of nanoparticle size on in vivo pharmacokinetics and cellular interaction, Nanomedicine 11 (2016) 673–692.
[14] M. Shilo, et al., The effect of nanoparticle size on the probability to cross the blood-brain barrier: An in-vitro endothelial cell model, J. Nanobiotechnology 13 (2015) 1–7.
[15] L. Gloag, et al., Zero valent iron core-iron oxide shell nanoparticles as small magnetic particle imaging tracers, Chem. Commun. 56 (2020) 3504–3507.
[16] L.M. Bauer, S.F. Situ, M.A. Griswold, A.C.S. Samia, High-performance iron oxide nanoparticles for magnetic particle imaging-guided hyperthermia (hMPI), Nanoscale 8 (2016) 12162–12169.
[17] T.H. Shin, et al., A magnetic resonance tuning sensor for the MRI detection of biological targets, Nat. Protoc. 13 (2018) 2664–2684.
[18] C. Bárcena, et al., Zinc ferrite nanoparticles as MRI contrast agents, Chem. Commun. 2224–2226 (2008), https://doi.org/10.1039/b801041b.
[19] L. Gloag, M. Mehdipour, D. Chen, R.D. Tilley, J.J. Gooding, Advances in the Application of Magnetic Nanoparticles for Sensing, Adv. Mater. 31 (at 2019,) 1–26, https://doi.org/10.1002/adma.201904385.
[20] S. Zhu, X. Xu, R. Rong, B. Li, X. Wang, Evaluation of zinc-doped magnetite nanoparticle toxicity in the liver and kidney of mice after sub-chronic intragastric administration, Toxicol. Res. (Camb) 5 (2015) 97–106.
[21] R.M. Borade, S.B. Somvanshi, S.B. Kale, R.P. Pawar, K.M. Jadhav, Spinel zinc ferrite nanoparticles: an active nanocatalyst for microwave irradiated solvent free synthesis of chalcones, Mater. Res. Express 7 (2020).
[22] D. Eberbeck, F. Wiekhorst, S. Wagner, L. Trahms, How the size distribution of magnetic nanoparticles determines their magnetic particle imaging performance, Appl. Phys. Lett. 98 (2011).
[23] S. Ota, et al., Effects of size and anisotropy of magnetic nanoparticles associated with dynamics of easy axis for magnetic particle imaging, J. Magn. Magn. Mater. 474 (2019) 311–318.
[24] N. Dogan, et al., Manganese doped-iron oxide nanoparticles and their potential as tracer agents for magnetic particle imaging (MPI), J. Magn. Magn. Mater. 561 (2022).
[25] Z. Jiang, et al., Mixed metal metal-organic frameworks derived carbon supporting znfe2o4/c for high-performance magnetic particle imaging, Nano Lett. 21 (2021) 2730–2737.
[26] N. Dogan, G. Caliskan, M. Irfan, Synthesis and characterization of biocompatible ZnFe2O4 nanoparticles for magnetic particle imaging (MPI), J. Mater. Sci. Mater. Electron. 34 (2023) 1–18.